Photodiagnosis and Photodynamic Therapy 28 (2019) 324–329

Contents lists available at ScienceDirect

Photodiagnosis and Photodynamic Therapy

journal homepage: www.elsevier.com/locate/pdpdt

Preparation and characterization of core-shell type Ag@SiO_2 nanoparticles for photodynamic cancer therapy

K.I. Dhanalekshmi[a,*], P. Magesan[b], K. Sangeetha[c], Xiang Zhang[a], K. Jayamoorthy[d], N. Srinivasan[e]

[a] School of Mechanical Engineering, Beijing Institute of Technology, Beijing, 100081, China
[b] Dept. of Chemistry, Bharath Institute of Higher Education & Research, Bharath University, Chennai, 600 073, Tamil Nadu, India
[c] Dept. of IBT, Bharath Institute of Higher Education & Research, Bharath University, Chennai, 600 073, Tamil Nadu, India
[d] Dept. of Chemistry, St. Joseph's College of Engineering, Chennai, Tamil Nadu, India
[e] Dept. of Chemistry, Pachiyappa's College for Men, Kanchipuram, 631501, Tamil Nadu, India

ARTICLE INFO

Keywords:
Photodynamic therapy
Photohemolysis
Core-shell nanoparticles
Stober's method
Characterization

ABSTRACT

With recent scientific developments, Photodynamic therapy (PDT) offers the promisie to become incorporated into the mainstream of cancer therapy. Noble metal based nano-PDT is increasing due to its advantages in the field of biomedicine. In this study, noble metal based Ag@SiO_2 core-shell nanoparticles were synthesized and to confirm the core-shell structure they were characterized by UV–vis, XRD, FTIR, TEM, and EDX. Our data confirm that core-shell type Ag@SiO_2 nanoparticles maintain its ability to kill cancer cells upon light irradiation. This shows that SiO_2 shell may not only prevent aggregation but it also may enhance the photodynamic activity of Ag nanoparticles.

1. Introduction

Photodynamic therapy (PDT) has emerged as an attractive treatment in clinical theranostic studies. Photodynamic therapy (PDT) acts on the anticancer tissues by generating reactive oxygen species in the presence of the photosensitizer (PS) [1].

PDT leads to the destruction of tumour cells by the two types of mechanisms. Type I reaction is based on the production of superoxide anion ($\cdot O_2^-$), hydroxyl radical (•OH), and hydrogen peroxide (H_2O_2). Type II reaction involves the generation of singlet oxygen ($^1O_2$). Initially, the photosensitizers (PS) in the ground state and it irradiated with the suitable wavelength of light commonly visible or near-infrared – excites the PS molecules. The light is selected on the criteria that the maximum absorption wavelength coincides with the PS molecules. The excited PS molecule reacts with the molecular oxygen present in the biological system and generates the highly toxic reactive oxygen species (ROS). This ROS can either destroy the tumour directly (Type II) [2–4] or kill the cancer cells either by apoptosis and necrosis, by inducing the damage in the tumor vasculature or through the enhancement of immunological effects (Type I) [5–7]. The three factors (PS, Light, and ROS) when combined is effective for tumor treatment.

Nanomedicine, in particular applications in PDT, may be superior to the conventional methods. The small size of the nanoparticles helps to achieve targeted therapy by targeting specific receptors and accumulating in pathological areas such as infarcted sites and hence enhancing the selectivity of the photodynamic therapy [1]. Vasculature in pathological areas is highly permeable and has enhanced retention effect (EPR) that results in the leaky nature being different in healthy tissues [8].

Plasmonic nanoparticles may have many advantages over organic photosensitizers. Gold and silver nanoparticles exhibit higher extinction coefficients, more stable, less prone to enzymatic degradation than organic photosensitizers [9,10]. Au, Ag and Cu nanoparticles exhibit strong surface plasmon resonance (SPR) bands in the visible region compared to other metals in the UV region [11–13]. Similarly, Ag shows largely red-shifted properties that contribute to the enhancement of anticancer activities in photodynamic cancer therapy. To increase the nanoparticles in the safety properties, they are encapsulated with semiconductor and hence the nanoparticles produced results in less toxic and biocompatible [14,15].

Silica nanoparticles are found to be promising in PDT applications [16–20] and have been examined in vitro and in vivo [21,22]. The encapsulation of photosensitizers with the silica nanoparticles is found to be very effective as silica is non-toxic, chemically inert and optically transparent. Chemical functionalization is enhanced due to the presence of hydroxyl groups on the silica surface [23,24]. Also, the combination of photosensitizers with stable silicon nanoparticles has been well absorbed by tumor cells and simultaneously degraded to eliminate

* Corresponding author.
E-mail address: dhanamveni88@gmail.com (K.I. Dhanalekshmi).

https://doi.org/10.1016/j.pdpdt.2019.10.006
Received 1 August 2019; Received in revised form 16 September 2019; Accepted 4 October 2019
Available online 07 October 2019
1572-1000/

in the form of silicic acid [25].

Hence in this study, core-shell type Ag@SiO_2 nanoparticles had been synthesized by Stober's method followed by the spectral characterization. Photodynamic activity of the synthesized nanoparticles was studied in the presence of the photosensitizers and light dose against the HeLa cells.

2. Materials and methods

2.1. Reagents

Silver nitrate ($AgNO_3$), tetraethyl orthosilicate (TEOS, 98%), ethanol (C_2H_5OH- 99.5%), Ammonium hydroxide (NH_4OH (25% NH_3)) and formaldehyde (HCHO) were purchased from Sigma-Aldrich. During the synthesis, Milli-Q water was used.

2.2. Synthesis of silica nanoparticles

Silica nanoparticles were successfully synthesized by the Stober's process. Comparing to the other methods, Stober's process is easy an eco-friendly method. The solution I (18 ml of ethanol and 6 ml TEOS) was added dropwise to the solution II (42 ml of ethanol and 9 ml of NH_4OH) under constant stirring. The speed of the titration was controlled at 20 s per droplet. After complete the titration, the mixture was constantly stirred for 1 h. Finally, the silica colloid was obtained which was aged for 1 day and no purification treatment was carried out.

2.3. Synthesis of Ag@SiO_2 core-shell nanoparticles

0.3 mmol of $AgNO_3$ was mixed with water and ethanol in the ratio of 1:9. To this solution add one day aged silica colloid (7.5 ml) with constant stirring. Added dropwise the ethanol solution with formaldehyde and controlled the titration speed by 14 s per droplet under constant stirring. The solution turned into a yellow colour. The obtained yellow solution was allowed to aged for 1 day and centrifuged to remove residual reactants. Finally the precipitate was washed with water.

2.4. Characterization

The absorption spectra were carried out using Perkin Elmer Lambda 35 spectrophotometer. XRD analysis was studied using X'pert PRO PANalytical diffractometer operated with Cu$K\alpha$ radiation (k = 1.5406 Å) source. FT-IR analysis was carried out RXI spectrometer in the 4000 – 500 cm^{-1} wave-number range using KBr pellets. TEM images were taken from a JEOL JEM-3010 electron microscope with the magnification of 600 and 800 k times operated at 300 keV.

2.5. Photohemolysis

2.5.1. Erythrocyte separation

Fresh human blood from healthy volunteers was collected and mixed with anticoagulant EDTA in ratio 3:1. After sometimes the erythrocytes were sediment at the bottom and finally, the leukocytes and thrombocytes were separated from the supernatant by gentle aspiration. The left out plasma was removed by washing the sediment 5–6 times with PBS. 0.5% erythrocyte suspension was prepared by adding 38 ml of PBS to the 2 ml of erythrocyte solution

2.5.2. Preparation of phosphate buffered saline (PBS)

PBS was prepared by the addition of 280 ml of 0.2 M monobasic sodium phosphate, 720 ml of 0.2 M dibasic sodium phosphate along with 9 g of sodium chloride and the pH recorded as 7.3. Subsequently, the solutions used in the assays were prepared in PBS.

2.5.3. Sample irradiation

The wavelength of light from the LED source used for the sample irradiation was 410 nm. About 1 ml of the nanoparticles at different concentrations were used and subjected to irradiation at different fluencies. The cell suspension was centrifuged at 1500 rpm for 10 min and the supernatant was measured using a spectrophotometer at 413 nm to quantify the percentage hemolysis.

The role of scavengers such as sodium azide (NaN_3) [26] and Glutathione reduced (GSH) [27] was studied by the above procedure using 1 ml of each scavenger separately with 1 ml of nanosensitizer in PBS.

2.5.4. Calculation of percentage of hemolysis

To compensate for the natural lysis of erythrocytes with time, a control sample (erythrocyte + PBS) was also included in the study. The above procedure was repeated for various concentrations and light doses for the synthesized nano photosensitizers. From the data, the percentage of hemolysis is calculated using the formula.

$$\%\text{of Hemolysis} = \frac{O.D_{exp} - O.D_{cs}}{O.D_{100\%}} \times 100$$

Where,

$O.D_{exp}$ = Optical density of the exposed sample

$O.D_{cs}$ = Optical density of the control sample

$O.D_{100\%}$ = Optical density of the 100% hemolysed solution

Control solution = 1.0 ml of erythrocyte suspension + 2.0 ml of PBS

100% Hemolysed solution = 1.0 ml of erythrocyte suspension + 2.0 ml of distilled water.

The graphs were plotted between the percentage of hemolysis and different concentrations and also for different fluences.

2.6. Cell culture

The human cervical cancer cell line (HeLa) procured from National Centre for Cell Science (NCCS), Pune were maintained in Eagles Minimum Essential Medium (EMEM) containing 10% fetal bovine serum.

The confluent HeLa cells (2×10^4 HeLa cells/ml) grown in 96 well plate maintained at 37 °C with 5% CO_2 were treated with nanoparticles at different concentrations and incubated for 3 h. Control cells were maintained parallel without adding the nanoparticles. Media containing compounds from the wells were removed and washed gently with PBS. Then illuminated the cells with different light doses using an LED light source and complete culture medium was added and incubated for 16 h.

2.7. MTT assay

Cell viability of the HeLa cells had been evaluated using MTT assay after 16 h. MTT was dissolved in PBS (5 mg/ml) and 10 µl was added to respective wells and incubated for 4 h. The resultant formazan crystals were dissolved in dimethyl sulfoxide (200 µl) and the absorbance intensity was measured at 570 nm [28–31].

$$\%\text{of Cell viability} = \frac{\text{Absorbance of the irradiated sample}}{\text{Absorbance of the Control}} \times 100$$

2.8. Statistical analysis

The datas were analyzed by two way analysis of variance (Annova) followed by Bonferroni post test using Graphpad Prism software V 4.00. The P Value lower than 0.05 were considered statistically significant. All the experiments were performed in triplicates and represented as the mean values with standard errors.

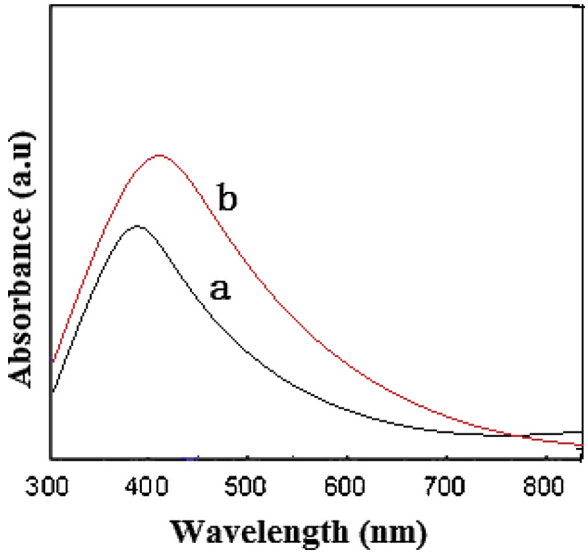

Fig. 1. Absorption spectrum of a) Ag NPs b) Ag@SiO_2 core-shell NPs.

3. Result and discussion

3.1. UV–vis spectral analysis

The UV–vis spectrum of free Ag nanoparticles and Ag@SiO_2 core-shell nanoparticles is shown in Fig.1 (a & b). The absorption spectrum of the Ag@SiO_2 core-shell NPs, the surface plasmon resonance (SPR) peak turned to the higher wavelength and located at 415 nm. The coating of SiO_2 over the Ag NPs which causes an enhance of SPR peak and red shifting was associated with decreased plasmon oscillation energy. When the silica shell cover the surface of Ag NPs exhibits a higher refractive index than Ag nanoparticles in water. Hence the peak of Ag@SiO_2 nanoparticles shifted to the higher wavelength [32–34]. The absorption spectrum shows a broader peak caused by the non-uniformity in the SiO_2 shell thickness and a different size of the NPs.

3.2. XRD analysis

The crystallographic structure was analyzed by powder X-ray diffractometer. The Fig.2 (a) shows that the air dried Ag@SiO_2 core-shell nanoparticles, strong and wide diffraction peak appeared in the XRD spectrum indicates the amorphous nature of SiO_2 and there is no peak corresponding to Ag. Fig.2 (b) shows the appearance of four distinct diffraction peaks at 38.10, 44.24, 63.92, 77.82° corresponding to the (111), (200), (220) and (311) which are typical of a face centered cubic structure of Ag. Using the Scherrer equation, the particle size was calculated as 35 nm. Equation [35] shows the Scherrer equation. In the equation, λ is the wavelength of the X-rays, β is the peak width in half of the maximum peak length (FWHM), and θ is the angle at which the most intense peak is seen [35].

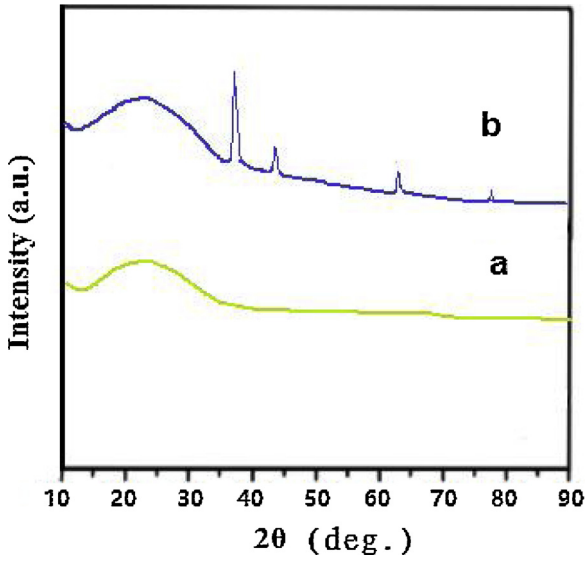

Fig. 2. XRD spectrum of Ag@SiO_2 core-shell NPs a) air dried sample and b) sample annealed at 650 ^{0}C.

$$\mathbf{d = 0.9\lambda/\beta \cos \theta}$$

3.3. FT-IR analysis

Fig. 3. shows the FT-IR spectrum of Ag@SiO_2 core-shell NPs. The band at about 3459 and 1656 cm^{-1} which represents the O—H stretching and bending vibrations of H_2O molecules. The two peaks at 1078 cm^{-1} and 961 cm^{-1} correspondings to the Si-O-Si and Si-O (H) asymmetric stretching vibrations and the peaks at 798 cm^{-1} and 463 cm^{-1} indicate the Si-O-Si symmetric stretching and bending vibrations respectively.

3.4. TEM & EDAX images

The particles size, morphology, and structure of the Ag@SiO_2 core-shell NPs are studied by using TEM images. Fig. 4 (a & b) shows the TEM images of Ag@SiO_2 core-shell nanoparticles. Their sizes distribute between 20–40 nm having an average of around 32 nm and shell thickness found to be 2–3 nm. The thickness of SiO_2 shell can be controlled by controlling the time of coating and TEOS concentration.

The elemental compositions of the Ag@SiO_2 NPs had been qualitatively determined by using energy dispersive X-ray (EDX) spectra and all the expected elements from the nanoparticle were observed. Fig. 5 shows the EDX spectrum of the Ag@SiO_2 core-shell particles which confirms the core-shell nanoparticle consists of core Ag and shell Si.

3.5. Photohemolysis

Photohemolysis is the rupture of red blood cell (RBC) membrane and the release of hemoglobin due to the exposure to light. in vitro photohemolysis of RBC is photosensitized by many other dyes and clinical drugs. It is used for the prediction of drugs that could photosensitize human skin. We have used photohemolysis of human erythrocytes as a model system in our study. The cell membrane disruption is studied and conveniently measured by photohemolysis [36]. Also, the ideal sensitizer should have not produced any cytotoxic effect on the healthy cells when added to the cellular suspension. The increase in the O.D at 413 nm represents the lysis (damage) of the erythrocytes.

The erythrocytes were irradiated as a function of light dose (fluence) is shown in the Fig. 6 (a). With the increasing concentration of Ag@SiO_2, the rate of photohemolysis also increased. At 25 μg/ml, the hemolysis was below 50% and attained the 50% hemolysis only at higher concentration.

The LD_{50} (Lethal Dose for 50% hemolysis) was found to be 84.75, 75.07, 52.34, 41.05 and 34.97 J/cm^2 for 50, 75, 100, 125 and 150 μg/ml concentration respectively. The increased concentration of the nanosensitizer also resulted in an increased hemolysis percentage at 150 μg/ml producing 97.1% hemolysis. In photohemolysis studies, the maximum hemolysis was achieved at 200 mg/ml (96.3%) for Au@SiO_2 core-shell nanoparticles [37], but in Ag@SiO_2 core-shell nanoparticles it was achieved at 150 mg/ml (97.1%). The results show that Ag@SiO_2 core-shell nanoparticle exhibits better photohemolysis activity than the Au@SiO_2 core-shell nanoparticles.

The erythrocytes irradiated as the function of the concentration of

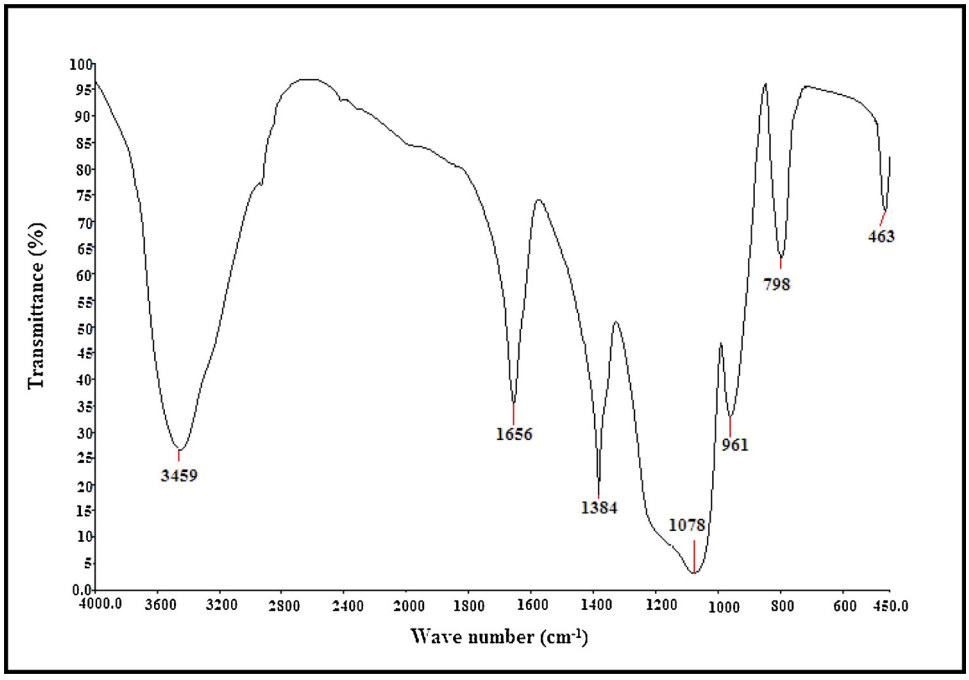

Fig. 3. FT-IR spectrum of Ag@SiO_2 core–shell NPs.

nanosensitizer are shown in Fig. 6 (b). Fig. 6 (b) clearly infers the photohemolysis increases with concentration as well as fluence. The LC_{50} (Lethal Concentration of NP for 50% hemolysis) was achieved only at 42.926, 57.235, 71.544, 85.853 J/cm^2 and not at the light dose 14.308, 28.617 J/cm^2. The LC_{50} values are 119.64, 91.30, 78.16, 48.95 μg/ml for light doses 42.926, 57.235, 71.544, 85.853 J/cm^2.

The results clearly signify that the increased concentration of sensitizers lessens the light dose requirement. Hence it is inferred that the nature of photohemolysis may be Type I or Type II mechanism.

The increased concentration of the nano-sensitizer also resulted in an increased hemolysis percentage at 150 μg/ml producing 97.1% hemolysis and at the statistical significance of *** $p > 0.001$

3.6. Effect of scavengers

As it is strongly suggested that photohemolysis depends on both drug and light dose and the nature of mechanism is purely chemical mediated one, it is also aimed to study whether the hemolysis is due to Type I/II mechanism. In order to know the mechanism of photohemolysis we carried out photohemolysis in the presence of scavengers such as GSH and NaN_3 which are the best known quenchers for superoxide anion and $^1O_2$ respectively. Fig.7. shows the role of scavenger GSH and NaN_3 for a different light dose at a fixed concentration of Ag@SiO_2 core-shell NPs. While the photohemolysis was carried through NaN_3, the photohemolysis was completely retarded due to the predominant singlet oxygen formation. However, superoxide anion formation was not sufficient which was substantiated by the invariable hemolysis percentage. Analysis of the effect of scavengers confirmed the dominant role of singlet oxygen formation over the superoxide anion which is quenched by NaN_3.

3.7. Cell viability

Cell viability assay was used to determine the cytotoxic concentration in HeLa cells in the presence of different nanoparticle concentrations at different light doses. Fig.8 (a) indicates the cell viability

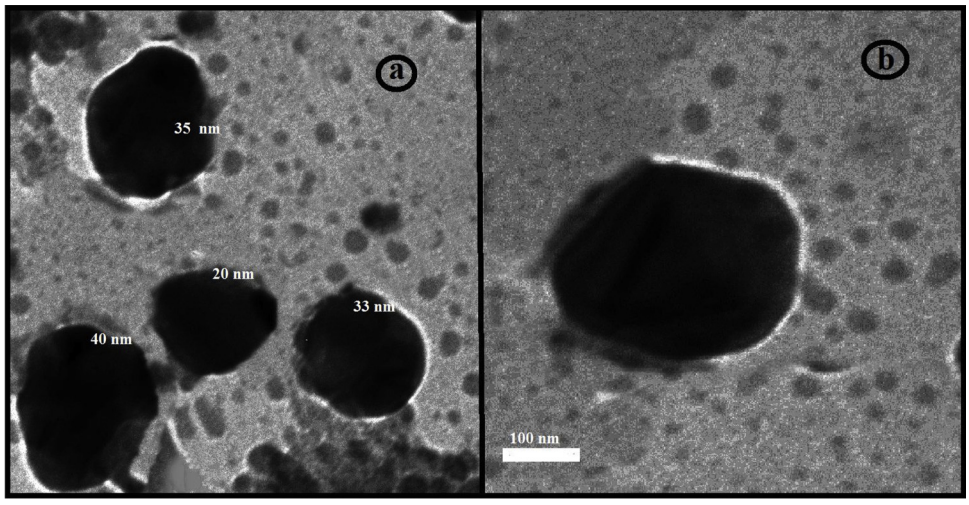

Fig. 4. (a & b) TEM images of Ag@SiO_2 core–shell NPs.

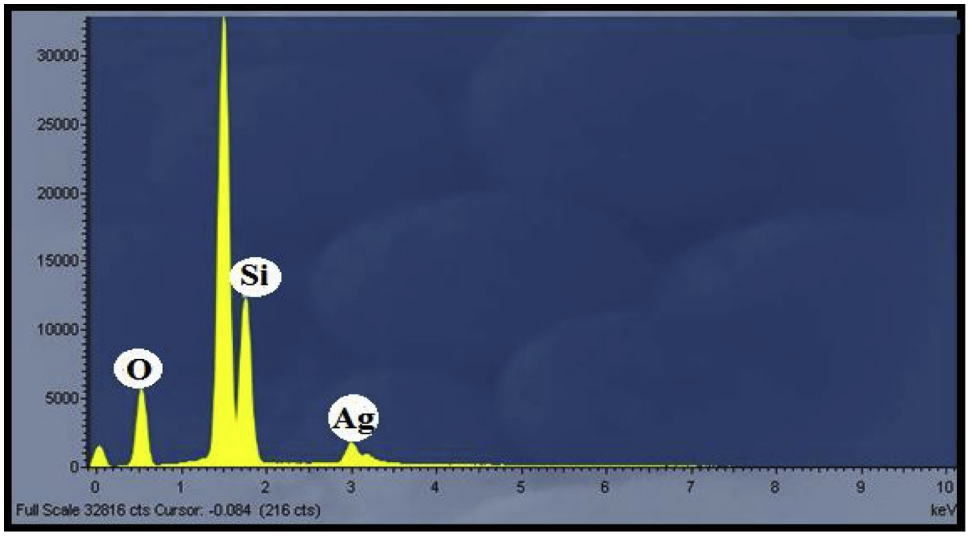

Fig. 5. EDX spectrum of Ag@SiO_2 core–shell NPs.

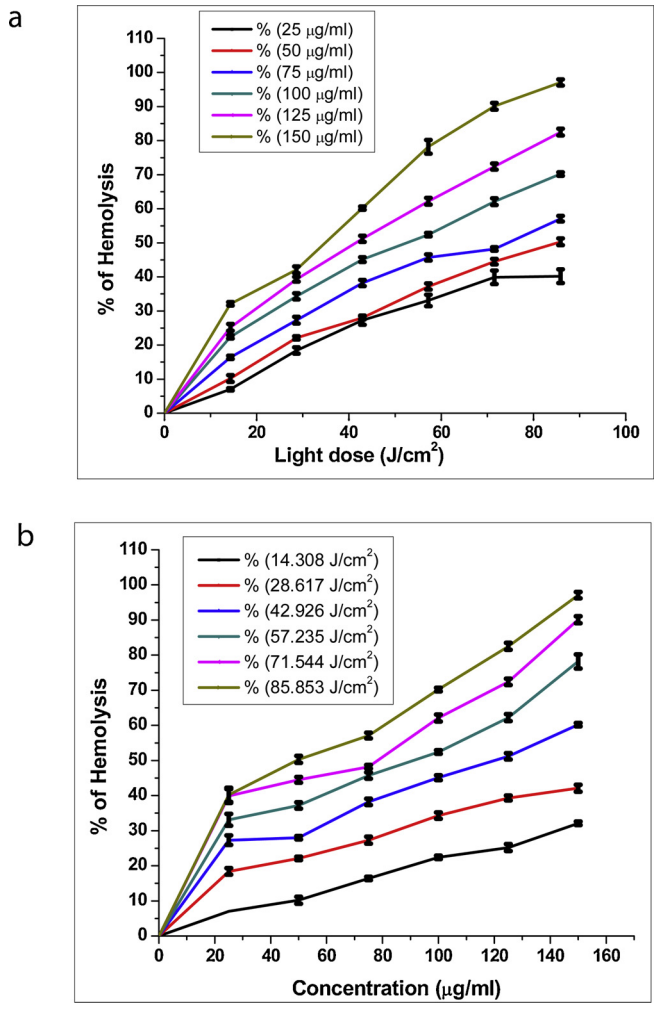

Fig. 6. (a) Effect of light dose on photohemolysis of Ag@SiO_2 core-shell NPs. Fig. 6 (b). Effect of concentration on photohemolysis of Ag@SiO_2 core-shell NPs.

variation along with the light dose. For the concentration of 50 µg/ml, the cell viability was lowered to 52% for 107.31 J/cm^2 of light dose. However, cell viability was decreased to 40 and 34% when the

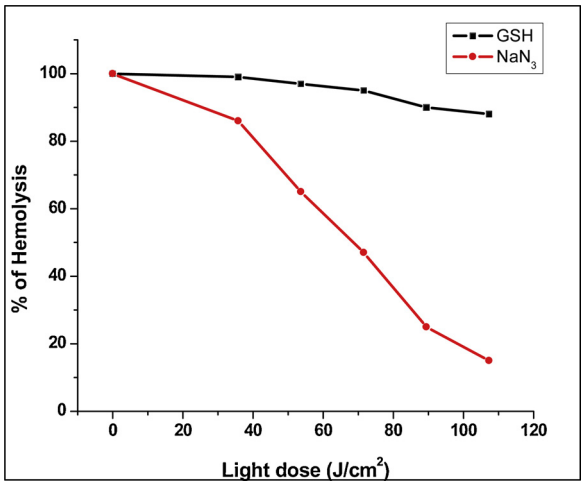

Fig. 7. Effect of scavengers on photohemolysis of Ag@SiO_2 core-shell NPs.

concentration was increased from 100 to150 µg/ml. At 200 µg/ml, the cell viability notably decreased and 85% of cancer cells growth was inhibited in the concentration for 107.31 J/cm^2 of light dose. LD_{50} was found to be 96.76, 72.02 and 47.97 J/cm^2 for 100, 150 and 200 µg/ml concentration respectively. The increased light dose and nanoparticle concentration increased the cytotoxic effects. Cell viability studies also show that cytotoxicity effect of Ag@SiO_2 core-shell nanoparticles is higher than the Au@SiO_2 core-shell nanoparticles.

From Fig. 8 (b), increased the light dose from 35.77 to 107.31 J/cm^2, significantly reduced the cell viability. At 107.31 J/cm^2 of light dose, the cell viability was reduced to 15% for 200 µg/ml. The LC_{50} was achieved only at 53.65, 71.54, 89.43 and 107.31 J/cm^2 and not in the 35.77 J/cm^2 of light dose. The LC_{50} values are 195.43, 150.63, 124.62 and 65.26 µg/ml for 53.65, 71.54, 89.43 and 107.31 J/cm^2. The results clearly infer that the increased sensitizer concentration reduces the light dose requirement to half.

4. Conclusion

In summary, Ag@SiO_2 core-shell NPs were successfully synthesized by the modified Stober's method. The SPR red shifting by absorption spectrum and powder XRD assays confirmed the encapsulation of Ag core with SiO_2 shell. Interaction of Ag core with SiO_2 shell was confirmed by FTIR results and further by TEM and EDX assays. Ag@SiO_2

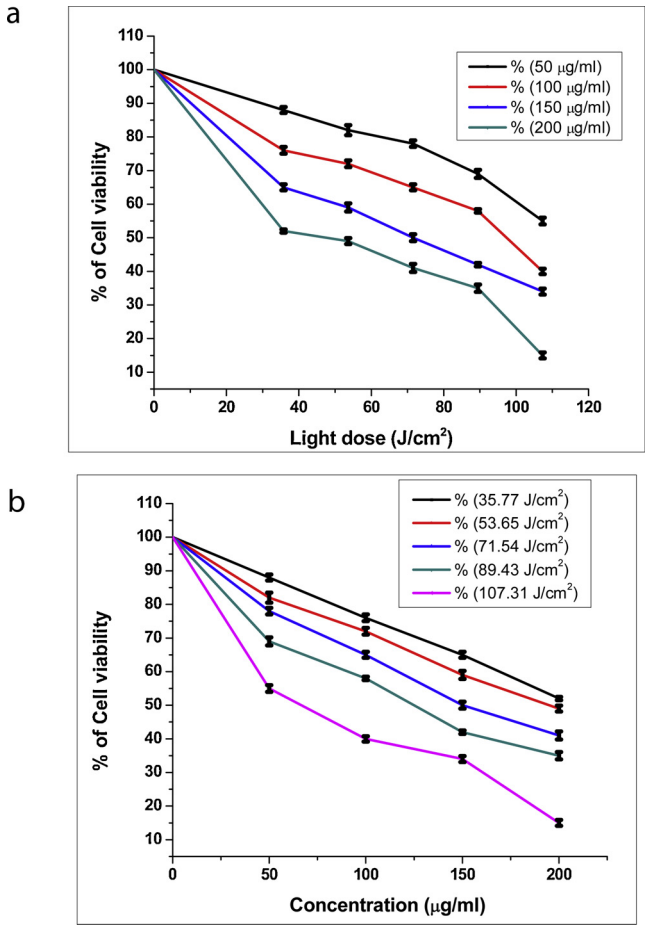

Fig. 8. (a). Effect of light dose on cell viability of $Ag@SiO_2$ core-shell NPs. Fig. 8 (b). Effect of concentration on cell viability of $Ag@SiO_2$ core-shell NPs.

NP_S had exhibited significant photohemolysis effect at the concentration of 150 μg/ml producing 97.1% hemolysis. The complete retardation of the photohemolysis by NaN_3 scavenger indicates the formation of singlet oxygen. Hence coating SiO_2 nanoparticle on the surface of Ag could enhance the photodynamic activity and could act as a suitable substitute for conventional photosensitizers such as organic dyes.

References

[1] S. Kwiatkowski, et al., Photodynamic therapy – mechanisms, photosensitizers and combination, Biomed. Pharmacother. 106 (2018) 1098–1107.
[2] W. Girotti, Photodynamic lipid peroxidation in biological systems, Photochem. Photobiol. 51 (1990) 497.
[3] Malik, T. Babushkin, S. Sher, J. Hanania, H. Ladan, Y. Nitzan, S. Salzberg, Collapse of K+ and ionic balance during photodynamic inactivation of leukemic cells, erythrocytes and Staphylococcus aureus, Int. J. Biochem. 25 (1993) 1399.
[4] J. Dougherty, C.J. Gomer, B.W. Henderson, G. Jori, D. Kessel, M. Korbelik, J. Moan, Q. Peng, Photodynamic therapy, J. Natl. Cancer Inst. 90 (1998) 889–905.
[5] V.H. Fingar, Vascular effects of photodynamic therapy, J. Clin. Laser Med. Surg. 14 (1996) 323.
[6] M.L. Agarwal, M.E. Clay, E.J. Harvey, H.H. Evans, A.R. Antunez, N.L. Oleinick, Photodynamic therapy induces rapid cell death by apoptosis in L5178Y mouse lymphoma cells, Cancer Res. 51 (1991) 5993.
[7] J. Webber, Y. Luo, R. Crilly, D. Fromm, D. Kessel, An apoptotic response to photodynamic therapy with endogenous protoporphyrin in vivo, J. Photochem. Photobiol. B 35 (1996) 209.
[8] V.P. Torchilin, Targeted pharmaceutical nanocarriers for cancer therapy and imaging, AAPS J. 9 (2007) E128–47.
[9] Jan Krajczewski, Karolina Rucinska, Helen E. Townley, Andrzej Kudelski, Role of various nanoparticles in photodynamic therapy and detection methods of singlet oxygen, Photodiagnosis Photodyn. Ther. 26 (2019) 162–178.
[10] Codruta Soica, et al., Silver-, gold-, and iron-based metallic nanoparticles: biomedical applications as theranostic agents for cancer, Design of Nanostructures for Theranostics Applications, (2018), pp. 161–242.
[11] M. Faraday, Preparation of colloidal gold, Philos Trans. 147 (1857) 145–181.
[12] J.A. Creighton, D.G. Eadon, Ultraviolet–visible absorption spectra of the colloidal metallic elements, J. Chem. Soc. Farad. Trans. 87 (24) (1991) 3881–3891.
[13] Qiaolin Wei YangyangLi, Xin Li FeiMa, Min Zhou FengyongLiu, Surface-enhanced Raman nanoparticles for tumor theranostics applications, Acta Pharm. Sin. B 8 (2018) 349–359.
[14] Xindong Wang, Hui Li, Guanying Chen, Core-Shell Nanostructures for Drug Delivery and Theranostics, Challenges, Strategies and Prospects for Novel Carrier Systems, (2018), pp. 143–175.
[15] T. Renjis, et al., Freely dispersible $Au@TiO_2$, $Au@ZrO_2$; $Ag@TiO_2$ and $Ag@ZrO_2$ core-shell nanoparticles: one-step synthesis, characterization spectroscopy and optical limiting properties, Langmuir 19 (2003) 3439–3445.
[16] P. Couleaud, V. Morosini, C. Frochot, S. Richeter, L. Raehm, J.O. Durand, Silica-based nanoparticles for photodynamic therapy applications, Nanoscale 2 (7) (2010) 1083–1095.
[17] M.R. Hamblin, Pinar Avci (Eds.), Applications of Nanoscience in Photomedicine (2015) 449-464.
[18] Peng Wang, Hong Tang, Peng Zhang, Plasmonic nanoparticle-based hybrid photosensitizers with broadened excitation profile for photodynamic therapy of cancer cells, Sci. Rep. 6 (2016) 34981.
[19] Yanyan Liu, Xianfu Meng, Bu Wenbo, Upconversion-based photodynamic cancer therapy, Coord. Chem. Rev. 379 (2019) 82–98.
[20] K.I. Dhanalekshmi, K.S. angeetha, K.S. Meena, P. Magesan, K. Jayamoorthy, Photodynamic activity and DNA binding studies of $Pd@SiO_2$ core-shell nanoparticles *in vitro*, Photodiagn. Photodyn. Ther. 26 (2019) 79–84.
[21] K. Wysocka-Król, A. Wieliczko, H. Podbielska, Silver doped nanomaterials and their possible use for antibacterial photodynamic activity, in: Hooman Mohseni, Massoud H. Agahi, Manijeh Razeghi (Eds.), Biosensing and Nanomedicine IV, vol. 8099, Proc. of SPIE, 2011809915-1-7.
[22] A. Liberman, N. Mendez, W.C. Trogler, A.C. Kummel, Synthesis and surface functionalization of silica nanoparticles for nanomedicine, Surf. Sci. Rep. 69 (2014) 132–158.
[23] X. He, X. Wu, K. Wang, B. Shi, L. Hai, Methylene blue-encapsulated phosphonate-terminated silica nanoparticles for simultaneous in vivo imaging and photodynamic therapy, Biomaterials. 30 (29) (2009) 5601–5609.
[24] B. Zhao, J.J. Yin, P.J. Bilski, C.F. Chignell, J.E. Roberts, Y. He, Enhanced photodynamic efficacy towards melanoma cells by encapsulation of Pc4 in silica nanoparticles, Toxicol. Appl. Pharmacol. 241 (2009) 163–172.
[25] L. Xiao, L. Gu, S.B. Howell, M.J. Sailor, Porous silicon nanoparticle photosensitizers for singlet oxygen and their phototoxicity against cancer cells, ACS Nano 5 (2011) 3651–3659.
[26] F. Wilkinson, J.G. Brummer, Rate constants for the decay and reactions of the lowest electrically excited singlet state of molecular oxygen in solution, J. Phys. Chem. Ref. Data 10 (1981) 809–999.
[27] K.N. Islam, Y. Kayanoki, H. Kaneto, K. Suzuki, M. Asahi, J. Fijii, N. Taniguchi, TGF-betal triggers oxidative modifications and enhances apoptosis in HIT cells through accumulation of reactive oxygen species by suppression of catalase and glutathione peroxidase, Free Radic. Biol. Med. 22 (1997) 1007–1017.
[28] T. Mossman, Rapid colorimetric assay for cellular growth and survival: application to proliferation and cytotoxicity assays, J. Immunol. Methods 65 (1983) 55–63.
[29] I. Roy, T.Y. Ohulchanskyy, H.E. Pudavar, et al., Ceramic-based nanoparticles entrapping water-insoluble photosensitizing anticancer drugs: a novel drug—carrier system for photody-namic therapy, J. Am. Chem. Soc. 125 (2003) 7860–7865.
[30] R.W.K. Wu, C.M.N. Yow, C.K. Wong, Y.H. Lam, Photodynamic therapy(PDT)-initiation of apoptosis via activation of stress-activatedp38 MAPK and JNK signal pathway in H460 cell lines, Photodiagn. Photodyn. Ther. 8 (2011) 254–263.
[31] E.S.M. Chu, C.M.N. Yow, Modulation of telomerase and signal trans-duction proteins by Hexyl-ALA-photodynamic therapy (PDT) inhuman doxorubicin resistant cancer cell models, Photodiagn. Photodyn. Ther. 9 (2012) 243–255.
[32] Haes, S.L. Zou, G.C. Schatz, R.P. Van Duyne, Nanoscale optical biosensor: short range distance dependence of the localized surface plasmon resonance of noble metal nanoparticles, J. Phys. Chem. B 108 (2004) 6961–6968.
[33] L.J. Sherry, R. Jin, C.A. Mirkin, G.C. Schatz, R.P. Van Duyne, Localized surface plasmon resonance spectroscopy of single silver triangular nanoprisms, Nano Lett. 6 (2006) 2060–2065.
[34] L.M. Liz-Marzán, M. Giersig, P. Mulvaney, Synthesis of nanosized gold− silica core− shell particles, Langmuir 12 (1996) 4329–4335.
[35] B.D. Cullity, Elements of X-ray Diffraction, Addison-Wesley Publishing Co.Inc., 1978.
[36] Davson, E. Ponder, Photodynamically induced cation permeability and itsrelation to haemolysis, J. Cell. Comp. Physiol. 15 (1940) 67–74.
[37] K.S. Meena, K.I. Dhanalekshmi, K. Jayamoorthy, Study of photodynamic activity of $Au@SiO_2$ core-shell nanoparticles in vitro, Mater. Sci. Eng. C 63 (2016) 317–322.